JOURNAL OF AIRCRAFT
Vol. 29, No. 6, Nov.–Dec. 1992

# Spinning Mode Analysis of the Acoustic Field Generated by a Turboshaft Engine

D. Blacodon* and S. Lévy†
*Office National d'Etudes et de Recherches Aérospatiales (ONERA), 92322 Châtillon, France*

**The spinning mode analysis of a ducted acoustic field is a powerful means for advancing the understanding of noise sources in turbofan or turboshaft engines, and it is also the main information needed to predict the far-field directivity radiated by the inlet or the nozzle. Tests were made with a circular array of fixed microphones in a nozzle cross section of a Turbomeca TM 333 turboshaft engine to determine the modal characteristics of its acoustic field. The main difficulty in data processing comes from the high background noise due to the very turbulent internal flow. A conventional method based on the angular Fourier transform of the cross-spectral matrix may therefore be inadequate. Several improvements are discussed and validated by numerical simulations, such as the use of a three-signal coherence technique to reduce the output noise. A further gain is achieved by the reduction of the estimate bias due to the finite number of statistical averages. The experimental TM 333 wave-number spectra are presented in the last section at several frequencies, corresponding to the broadband combustion noise and to the tones emitted by the high-pressure turbine and the free turbine. The observed spinning modes are explained by taking into account the nozzle cut-off properties and the radiation mechanisms of transonic rotors.**

## I. Introduction

TURBOSHAFT engines may be the main contribution to helicopter external noise at takeoff or even in approach. This was clearly found with weighted units, such as dBA or PNdB.[1–3] Noise prediction and reduction is one of the prime challenges for engine manufacturers. The spectrum and directivity measurements of the sound field radiated by the inlet or the nozzle are of primary importance. They are, however, insufficient to better understand the generation mechanisms. A previous study using three-signal coherent spectra enabled us to separate the various internal noise sources and to determine the frequency band emitted by each of them.[3–5]

The spatial structure of the acoustic field radiated at each frequency is of interest for two main reasons[6]:

1) The spinning modes give more information on the tones generated, because they are related to the symmetries of the compressor or turbine rotors and stators.

2) The free-field directivity is strongly dependent on the cutoff ratio, which is a function of the frequency and mode.

Angular wave-number spectra have been measured by others[7–9] in turbofan engines, with a moving microphone and a fixed one used as phase reference. Some applications of this approach are presented in Ref. 10 using a Société Nationale d'Etude et de Construction de Moteurs d/Aviation (SNECMA) test bench. This kind of method is generally not well suited to the study of turboshaft engines because their sizes are small and the duct cross sections may be not perfectly circular.

Progress in data processing computers made it possible to implement alternate approaches.[11–14] They consist of replacing the angular scanning by an array of fixed microphones. The main drawback of this technique is the spatial sampling of the sound field.[15] According to Nyquist's theorem, the number of microphones must be at least twice as high as the highest-occurring spinning mode. All the microphones must also be accurately calibrated to avoid spurious spinning modes in the results. There are, of course, some advantages over the previous methods, because the measurements are made simultaneously in all locations. This greatly reduces the duration of a run, and a better time average is obtained.

Another problem in such experiments is the background noise (e.g., the flow noise on the probes) which can be rather high compared with the acoustic field. It is shown in the next section that the output background noise can only be reduced by increasing the number of microphones with conventional data processing based simply on time and angular Fourier transforms. Some acoustic spinning modes may then be overwhelmed by spurious modes. The objective of this paper is to present more sophisticated techniques that solve this difficulty by improving the output signal-to-noise ratio. These methods are compared in Sec. III, and they are validated by numerical simulations. They are applied in Sec. IV to tests performed in May 1986 in the Turbomeca open-air facility at Pau-Uzein, where a cross section of the nozzle of a Turbomeca TM 333 turboshaft engine was equipped with eight flush-mounted probes, every 45 deg.

## II. Conventional Data Processing for Calculating the Angular Wave-Number Spectra

### A. General Equations

The time signal $y(t, \theta)$ measured by a probe at angle $\theta$ is written

$$y(t, \theta) = s(t, \theta) + n(t, \theta) \tag{1}$$

where $s(t, \theta)$ is the acoustic pressure and $n(t, \theta)$ is the background noise. The Fourier transform in the frequency domain is

$$Y(f, \theta) = S(f, \theta) + N(f, \theta) \tag{2}$$

The angular Fourier series of $Y(f, \theta)$ is

$$\mathcal{Y}(f, m) = \mathcal{S}(f, m) + \mathcal{N}(f, m) \tag{3a}$$

Presented as Paper 90-4012 at the AIAA 13th Aeroacoustics Conference, Tallahassee, FL, Oct. 22–24, 1990; received Nov. 26, 1990; revision received Dec. 3, 1991; accepted for publication Dec. 4, 1991.

*Research Scientist, Physics Department, BP72. Member AIAA.
†Deputy Head of Acoustics Division, Physics Department, BP72. Member AIAA.

where $m$ (integer) is the angular wave-number, or spinning mode. There is no simple relation between $\mathcal{Y}(f, -m)$ and $\mathcal{Y}(f, +m)$ since $Y(f, \theta)$ is complex. The wave-number spectrum is the power spectral density (PSD)

$$\phi(f, m) = |\mathcal{Y}(f, m)|^2 = \mathcal{Y}(f, m) \cdot \mathcal{Y}^*(f, m) \quad (3b)$$

where * denotes the complex conjugate.

The signals are only measured in $J$ locations $\theta_j = 2\pi(j - 1)/J$, with $j = 1, 2, \ldots, J$ (Fig. 1). Then

$$\mathcal{Y}(f, m) = \frac{1}{J} \sum_{j=1}^{J} Y(f, \theta_j) \cdot \exp(im\theta_j) \quad (4a)$$

$$\phi(f, m) = \frac{1}{J^2} \sum_{j=1}^{J} \sum_{j'=1}^{J} Y(f, \theta_j) \cdot Y^*(f, \theta_{j'}) \cdot \exp(im\theta_j) \cdot \exp(-im\theta_j) \quad (4b)$$

Moreover, a subscript $\ell$ should be introduced in all the above notations because the Fourier transforms are computed on a data block $(\ell - 1)T < t < \ell T$, where $T$ is greater than the maximum period under study (the frequency resolution is $\Delta f = 1/T$). The signals are assumed to be stationary, and the results are thus statistically averaged by the relation

$$\Phi(f, m) = \langle \phi_\ell(f, m) \rangle = \lim_{L \to \infty} \frac{1}{L} \sum_{\ell=1}^{L} \phi_\ell(f, m) \quad (5)$$

where $\phi_\ell(f, m)$ is given by Eq. (4b). $\Phi(f, m)$ is plotted vs $m$ for each frequency $f$, of interest. Contrary to a frequency spectrum, the positive and negative values of $m$ must be distinguished according to the remark following Eq. (3a).

The matrix notation is more convenient for further development. It is based upon the cross-spectral matrix

$$\Gamma(f) = \begin{bmatrix} Y_{11}(f) & \ldots & Y_{1J}(f) \\ Y_{21}(f) & \ldots & Y_{2J}(f) \\ \vdots & \ldots & \vdots \\ Y_{J1}(f) & \ldots & Y_{JJ}(f) \end{bmatrix} \quad (6)$$

with $Y_{jj'}(f) = \langle Y_\ell(f, \theta_j) \cdot Y_\ell^*(f, \theta_{j'}) \rangle$.

The final relation of Eq. (5) is then

$$\Phi(f, m) = \boldsymbol{U}^+ \cdot \Gamma(f) \cdot \boldsymbol{U} \quad (7)$$

where $\boldsymbol{U}$ is the column matrix

$$\boldsymbol{U} = \frac{1}{J} \begin{bmatrix} \exp(im\theta_1) \\ \exp(im\theta_2) \\ \vdots \\ \exp(im\theta_J) \end{bmatrix}$$

and the superscript + denotes the transposed complex conjugate.

### B. Signal-to-Noise Ratio

The number of microphones, $J$, is the most important parameter because of spatial aliasing (Nyquist's theorem). Modes $m$ are computed in the range $(-J/2, +J/2 - 1)$ if $J$ is even, and are defined modulo $J$ (for instance, modes $-J$, 0, $J$, $2J$, . . . are found as a single line at $m = 0$).

The value of $J$ also determines the signal-to-noise ratio $(S/N)$ of the method. Two general hypotheses are assumed herein:

1) The acoustic field and the background noise are statistically independent

$$\langle S_\ell(f, \theta_j) \cdot N_\ell^*(f, \theta_j) \rangle = 0 \quad (8)$$

2) The background noises in two different locations are also statistically independent, which means that the spacing between successive probes is sufficiently large

$$\langle N_\ell(f, \theta_j) \cdot N_\ell^*(f, \theta_{j'}) \rangle = \sigma_j^2 \cdot \delta_{jj'} \quad (9)$$

where $\delta_{jj'}$ is the Kronecker symbol and $\sigma_j^2$ the noise PSD at $\theta_j$. Note that this PSD may depend on the angle, $\theta_j$, of each probe.

Taking these two hypotheses into account, the cross-spectral matrix is written

$$\Gamma(f) = \Gamma_S(f) + \Gamma_N(f) \quad (10)$$

where $\Gamma_s(f)$ looks like $\Gamma(f)$ with $S_{jj'}(f) = \langle S_\ell(f, \theta_j) \cdot S_\ell^*(f, \theta_{j'}) \rangle$ instead of $Y_{jj'}(f)$, and $\Gamma_N(f)$ is a diagonal matrix

$$\Gamma_N(f) = \begin{bmatrix} \sigma_1^2 & 0 & 0 \ldots & 0 \\ 0 & \sigma_2^2 & 0 \ldots & 0 \\ \ldots & \ldots & \ldots & \ldots \\ \ldots & \ldots & \ldots & \ldots \\ 0 & 0 & \ldots 0 & \sigma_J^2 \end{bmatrix} \quad (11)$$

The input $S/N$ is

$$(S/N)_{IN} = \frac{Tr[\Gamma_S(f)]}{Tr[\Gamma_N(f)]} \quad (12)$$

where $Tr[\ldots]$ is the trace of the matrix. After data processing, the output $S/N$ is

$$(S/N)_{OUT} = \frac{\Phi_S(f, m)}{\Phi_N(f, m)} \quad (13)$$

with $\Phi_N(f, m) = \boldsymbol{U}^+ \cdot \Gamma_N(f) \cdot \boldsymbol{U} = (1/J^2) \cdot Tr\,[\Gamma_N(f)]$.

The gain in $S/N$ is defined as

$$G(f, m) = \frac{(S/N)_{OUT}}{(S/N)_{IN}} = J^2 \cdot \frac{\Phi_S(f, m)}{Tr[\Gamma_S(f)]} \quad (14a)$$

If there is only a single mode, $m$, then $Tr(\Gamma_S(f)] = J \cdot \Phi_S(f, m)$, and

$$G = J \quad \text{or} \quad 10 \cdot \log G = 20 \cdot \log \sqrt{J} \quad \text{in dB} \quad (14b)$$

which is the conventional result of an improvement of $S/N$ by a factor $J$ for coherent data processing with the signals of $J$ probes.

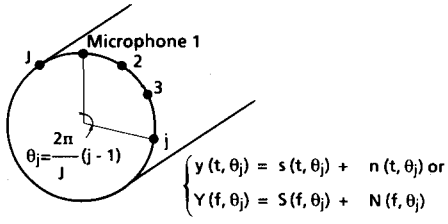


**Fig. 1 Array of fixed equidistant microphones for spinning mode analysis.**

### C. Numerical Simulation

Numerical simulations were used to verify the theoretical equations and to test the data processing. Let us consider an acoustic field, $s(t, \theta)$, which is a single frequency $f = 1$ kHz consisting of three spinning modes at different levels: 1) $m = +2$ (100 dB); 2) $m = -4$ (90 dB); and 3) $m = +5$ (70 dB). The white noise level, $n(t, \theta)$, is assumed to be 95 dB in each frequency band $\Delta f$ (here $\Delta f = 31$ Hz) in every location $\theta_j$, i.e. $10 \cdot \log (S/B)_{IN} = 5$ dB for the most intense mode. The mode $m = -4$ is only 5 dB under the background noise, but $m = +5$ is 25 dB under it. With $J = 24$ measurement locations, the wave-number spectra are computed in the range

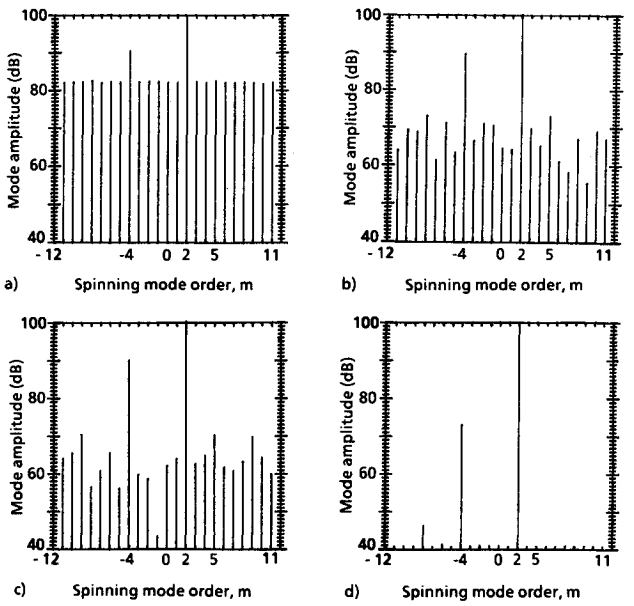


**Fig. 2 Numerical simulation of three spinning modes: $f$ = 1 kHz, $m$ = +2 (100 dB), $m$ = −4 (90 dB), and $m$ = +5 (70 dB); background noise 95 dB. Wave-number spectra at 1 kHz: $J$ = 24 probes; $L$ = 100 statistical averages: a) conventional method, Eq. (7); b) data processing based on Eq. (17); c) data processing based on Eq. (22); and d) data processing based on Eq. (24).**

$-12 \leqslant m \leqslant +11$. All the results are averaged on $L = 100$ successive data blocks.

The wave-number spectrum at 1 kHz is displayed in Fig. 2a. The three modes are recovered with their exact levels. However, the lowest one, $m = +5$, is totally buried in the background noise, that is well predicted by (14b)

$$10 \cdot \log(S/N)_{\text{OUT}} \simeq 10 \cdot \log(S/N)_{\text{IN}} + 10 \cdot \log J = 19 \text{ dB}$$

It would be very difficult to greatly improve the output $S/N$ with this conventional method, because twice as many microphones would only increase $(S/N)_{\text{OUT}}$ by 3 dB (and $J$ = 24 is already rather large). For this reason, other data processing techniques must be developed to obtain useful results in actual tests.

## III. Improved Methods of Wave-Number Spectrum Analysis

### A. Cancellation of the Diagonal Noise Terms in the Cross-Spectral Matrix

Since the noise matrix [Eq. (11)] is diagonal, the first idea is to eliminate these terms from the cross-spectral matrix [Eqs. (6) and (10)] by a three-signal coherence technique.[5,16] Let us consider the signals measured at angles $\theta_j$, $\theta_k$, and $\theta_n$

$$Y_\ell(f, \theta) = S_\ell(f, \theta) + N_\ell(f, \theta), \quad \text{for} \quad \theta = \theta_j, \theta_k \quad \text{and} \quad \theta_n$$

The coherent diagonal terms of the cross-spectral matrix are

$$Y^c_{jj}(f) = \frac{Y_{jk}(f) \cdot Y_{nj}(f)}{Y_{nk}(f)} \tag{15}$$

Taking into account the hypotheses of Eqs. (8) and (9), they can be written

$$Y^c_{jj}(f) = \frac{S_{jk}(f) \cdot S_{nj}(f)}{S_{nk}(f)} \tag{16}$$

It appears that the noise is clearly eliminated. The cross-spectral matrix $\Gamma^c(f)$ is deduced from $\Gamma(f)$ by changing the $Y_{jj}(f)$ into $Y^c_{jj}(f)$on the diagonal. Equation (7) then becomes

$$\Phi^c(f, m) = \boldsymbol{U}^+ \cdot \Gamma^c(f) \cdot \boldsymbol{U} \tag{17}$$

The above equations are easily demonstrated to be valid if there is only one acoustic mode, $m$. It is shown in Fig. 2b that they are also valid if several modes occur. Practically, it must be verified that Eq. (16) is independent of the choice of the two measurement locations $\theta_k$ and $\theta_n$. The result of the numerical simulation (Fig. 2b) shows that background noise is not completely eliminated as expected, but is reduced by about 10 dB compared with Fig. 2a. It is on the same order as the level of $m = +5$.

The explanation is as follows. The statistical averages as in Eq. (5) should be made on an infinite number of data blocks instead of a limited number (here $L = 100$). In this case, the cross-spectral matrix $\Gamma(f)$ in Eq. (6) is only known by its estimate $\hat{\Gamma}(f)$, with

$$\hat{Y}_{jj'}(f) = \langle Y_\ell(f, \theta_j) \cdot Y^*_\ell(f, \theta_{j'}) \rangle_L \tag{18}$$

Relations in Eqs. (8) and (9) are not strictly valid if the averages are limited to $L$, and

$$\hat{Y}_{jj'}(f) = \langle S_\ell(f, \theta_j) \cdot S^*_\ell(f, \theta_{j'}) \rangle_L + \langle N_\ell(f, \theta_j) \cdot N^*_\ell(f, \theta_{j'}) \rangle_L + \langle S_\ell(f, \theta_j) \cdot N^*_\ell(f, \theta_{j'}) \rangle_L + \langle N_\ell(f, \theta_j) \cdot S^*_\ell(f, \theta_{j'}) \rangle_L \tag{19}$$

Because the general background noise has been removed, the diagonal and nondiagonal noise terms, previously negligible, now become predominant. They generate estimate errors in the cross-spectral densities $Y_{jj'}(f)$, equal to the variance

$$\sigma^2_Y = \langle |\hat{Y}_{jj'}(f) - Y_{jj'}(f)|^2 \rangle$$

If the background noise is "spatially white" ($\sigma^2_1 = \sigma^2_2 = \ldots \sigma^2_j = \sigma^2$), and if its PSD is high, it is found that

$$\sigma^2_{\hat{Y}} \simeq \sigma^2 / \sqrt{L}$$

The estimate errors in $Y^c_{jj}(f)$ are on the same order as those in $Y_{jj'}(f)$ since the $Y^c_{jj}(f)$ are deduced from the $\hat{Y}_{jj'}(f)$. The noise PSD is thus divided by $\sqrt{L}$, and the gain in $S/N$ given in Eq. (14b) is multiplied by $\sqrt{L}$

$$G^c = J \cdot \sqrt{L} \quad \text{or} \quad 10 \cdot \log G^c = 10 \cdot \log(J \cdot \sqrt{L}) \tag{20}$$

The improvement of 10 dB in Fig. 2b is indeed equal to $10 \cdot \log \sqrt{L}$ with $L = 100$. A greater number of averages, $L$, only slightly increases $G^c$ because of the square root. A reduction of the nondiagonal noise terms would thus be needed for further gain in $S/N$.

### B. Decrease of the Nondiagonal Noise Terms in the Estimated Cross-Spectral Matrix

Let us first modify the structure of the matrix $\Gamma^c(f)$ line by line

$$\Gamma'^c(f) = \begin{bmatrix} \hat{Y}^c_{11}(f) & \hat{Y}_{12}(f) & \hat{Y}_{13}(f) & \ldots & \hat{Y}_{1J}(f) \\ \hat{Y}^c_{22}(f) & \hat{Y}_{23}(f) & \hat{Y}_{24}(f) & \ldots & \hat{Y}_{21}(f) \\ \vdots & \vdots & \vdots & \vdots & \vdots \\ \hat{Y}^c_{JJ}(f) & \hat{Y}_{J1}(f) & \hat{Y}_{J2}(f) & \ldots & \hat{Y}_{JJ-1}(f) \end{bmatrix}$$

or

$$\Gamma'^c(f) = \begin{bmatrix} \boldsymbol{V}_1(f) \\ \boldsymbol{V}_2(f) \\ \vdots \\ \boldsymbol{V}_J(f) \end{bmatrix} \tag{21}$$

Each line vector $\boldsymbol{V}_j$ contains the component at the frequency $f$ of the cross spectra between a reference signal $j$ and the signals at all the other locations $j' \neq j$. This is similar to the

data processing technique used with a fixed microphone and a moving probe, except that the continuous scanning of the sound field is spatially sampled here every $2\pi/J$.[10,17] It is shown in Ref. 17 that the wave-number spectrum is

$$\Phi_j^c(f, m) = \frac{|\boldsymbol{U}^+ \cdot \boldsymbol{V}_j(f)|^2}{\hat{Y}_{jj}^c(f)} \tag{22}$$

The numerical simulation is given in Fig. 2c. The result is quite similar to that of Fig. 2b, with approximately the same background noise level. This is not surprising since $(S/N)_{OUT}$ is again mainly determined by the errors due to the estimate of the cross-spectrum components (finite value of $L$), which are on the same order as in the previous section. The background noise is in fact slightly lower than in Fig. 2b, and only the highest noise components reach the level of $m = +5$. The limit of detection (about 70 dB) is thus 25 dB below the input noise (95 dB, see Sec. II.C.) in this example.

$(S/N)_{OUT}$ may be increased by taking the average of the $J$ vectors, $\boldsymbol{V}_j(f)$

$$\bar{V}(f) = \frac{1}{J} \sum_{j=1}^{J} \frac{\boldsymbol{V}_j(f)}{\sqrt{\hat{Y}_{jj}^c(f)}} \tag{23}$$

$\bar{V}(f)$ is a line matrix, each element of which is the mean value of the normalized elements in a column of $\Gamma'^c(f)$. With a single mode, it is easy to understand that the parts due to the acoustic field are coherently added (there is a phase relationship between them), and that the parts due to the noise are incoherently added, which reduces the noise variance by a factor $J$. Finally, instead of Eq. (22)

$$\Phi'(f, m) = |\boldsymbol{U}^+ \cdot \bar{V}(f)|^2 \tag{24}$$

and the value of $G^c$ in Eq. (20) is replaced by

$$G' = J \cdot G^c = J^2 \cdot \sqrt{L} \quad \text{or} \quad 10 \cdot \log G' = 10 \cdot \log(J^2 \cdot \sqrt{L}) \tag{25}$$

The wave-number spectrum in Fig. 2d shows a dramatic reduction of the background noise. The differences between Figs. 2c and 2d are slightly higher than $10 \cdot \log J = 14$ dB. However, only $m = +2$ is correctly recovered with a 100 dB level. The mode $m = -4$ also clearly appears but with the wrong level, and $m = +5$ is not found at all. The explanation has already been given in the comment after Eq. (23), which was based on the case of a single mode. When there are several modes, the phase shifts between the cross-spectrum components in each column of $\Gamma'^c(f)$ may be different and some modes may be more or less underpredicted in the averaged $\bar{V}(f)$ vector. In other words, these modes are processed as if they were noise.

It is well known that the more sophisticated the data processing, the more restrictive the hypotheses. According to the space structure of the acoustic field, some mode levels may be wrong and some modes may even disappear. As a consequence, this last method is well suited for identifying only the predominant modes. It may be very useful for determining what the actual acoustic sources are, by analyzing the symmetries of the compressor or turbine rotors and stators, or for predicting the shape of the far-field directivity pattern. However, in its present form, it cannot yet give any quantitative information on the acoustic levels.

Some modifications have been made to solve this problem. The idea is to first take the angular Fourier transform of each line vector $\boldsymbol{V}_j(f)$, before calculating any average. An acoustic mode has the same level in each computed wave-number spectrum, and therefore its mean value is also the same. On the contrary, this is not true for a background noise mode. A threshold tending to eliminate the noise can then be defined by comparing the averaged and nonaveraged levels of each mode. The initial results obtained in this way are very encouraging.

## IV. Spinning Mode Analysis in a Turboshaft Engine Nozzle

### A. Test Background

The methods presented in the previous sections are applied to tests performed in May 1986 in the Turbomeca open-air facility at Pau-Uzein.[18] A cross section of a nozzle of a Turbomeca TM 333 turboshaft engine (Fig. 3) was equipped with eight microphones, every 45 deg (Fig. 4). This number is obviously small, but the experiments are difficult due to the high-temperature flow (about 400°C). Thus, special devices, described in Refs. 4 and 5, had to be designed, with a small tube, a remote microphone, and a long coiled tube to prevent standing waves. A test at the takeoff power of twin-engine aircraft (460 kW or 620 HP) is discussed in this section. All the results are again obtained with $L = 100$ statistical averages.

A frequency spectrum on 5 kHz (resolution $\Delta f = 39$ Hz) measured by the first microphone ($j = 1$ in Fig. 4) is shown in Fig. 5. The main features are 1) the very loud broadband combustion noise around 300 Hz (it would seem to be lower in a third-octave analysis or in weighted units such as dBA, dBD or PNdB); and 2) several tones due to the gas generator high-pressure (HP) turbine rotation, $N_{HP} = 745$ Hz, or the free low-pressure (LP) power turbine rotation, $N_{LP} = 627$ Hz (see Fig. 3).

Since there are only $J = 8$ microphones, the modes are computed in the range $-4 \leq m \leq +3$. If other modes prop-

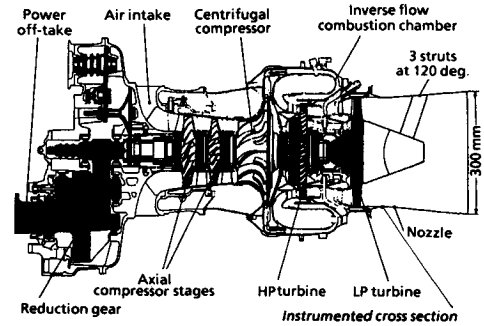


**Fig. 3 Schematic view of the Turbomeca TM 333 turboshaft engine.**

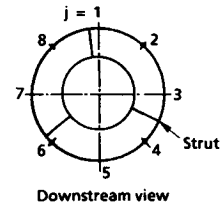


**Fig. 4 Locations of the microphone probes on the TM 333 nozzle wall, in the cross section marked in the previous figure (the three struts every 120 deg are located in a downstream section).**

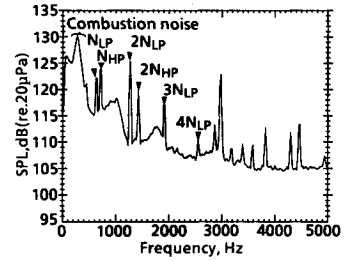


**Fig. 5 Frequency spectrum measured by microphone 1 in Fig. 4 (resolution of $\Delta f = 39$ Hz).**

agate, an aliasing problem appears. The cut-on frequency of a spinning mode $m$ in a circular duct with rigid walls is

$$f_c(m) = \sqrt{1 - M^2}\cdot(a\chi_m/2\pi R) \qquad (26)$$

where $a$ is the sound velocity, $R$ the duct radius, $M$ the flow Mach number inside the duct, and $\chi_m$ is the abscissa of the first maximum of the Bessel function of the first kind and of order $|m|$. If $m = 0$ then $\chi_m = 0$ and $f_c = 0$. For $m \geq 1$, it is found in treatises on Bessel functions that

$$\chi_m \simeq m + 0.8086\cdot m^{1/3} + 0.0725\cdot m^{-1/3} - 0.051\cdot m^{-1} + 0.0094\cdot m^{-5/3} + \ldots$$

A given mode $m$ is cut on at a frequency $f$ if $f \geq f_c(m)$, or the cut-on modes at a given frequency $f$ are such that $\chi_m < 2\pi Rf/(a\sqrt{1 - M^2})$, which means that only the values of $|m|$ lower than a limit, $m_c$, can propagate. In the TM 333 nozzle, with $D = 0.3$ m, $a = 520$ m/s (temperature 400°C) and $M = 0.3$

$$f_c(m) = 526\cdot\chi_m \quad \text{in} \quad \text{Hz}$$

There is no spatial aliasing up to $f_c(4) = 2.8$ kHz (above this value, $m = +4$ would alias into $m = -4$). The spectrum in Fig. 5 shows that most noise is emitted below this frequency. There is only a large tone at 3 kHz, the origin of which is not clearly identified.

The harmonics of the two shaft rotation speeds $N_{HP}$ and $N_{LP}$ are explained by the fact that the two turbine stages are transonic, and thus emit multiple pure tones.[19] The main noise source is then related to the mean blade aerodynamic loading. Only one mode is theoretically generated in each tone and is equal to the harmonic orer $f/N$ ($N$ stands for either $N_{HP}$ or $N_{LP}$). The cut-on condition of Eq. (26) becomes

$$f \geq f_c(m) \quad \text{or} \quad mN \geq \sqrt{1 - M^2}\cdot(a\chi_m/2\pi R)$$

hence

$$\frac{\chi_m}{m} \leq \frac{M_R}{\sqrt{1 - M^2}} \qquad (27)$$

where $M_R = 2\pi RN/a$ is the tip Mach number. The curve $\chi_m/m$ is plotted vs $m$ in Fig. 6. It appears that the first harmonics are cut off even with a supersonic tip speed. They are, however, observed in Fig. 5 because the noise sources are very strong, and because the nozzle is short and the measurements are made in an upstream section of the duct, i.e., near the acoustic sources. Since $f/f_c$ is not much lower than one, the decay rates of these cut-off modes are not very high and they can still be found at the microphone locations.

### B. Wave-Number Spectra

The wave-number spectra are computed in each frequency band $\Delta f = 39$ Hz (i.e., 128 curves up to 5 kHz) for $-4 \leq m \leq +3$. An example at a low frequency (combustion noise) is given in Fig. 7. The four methods are compared as in Fig. 2.

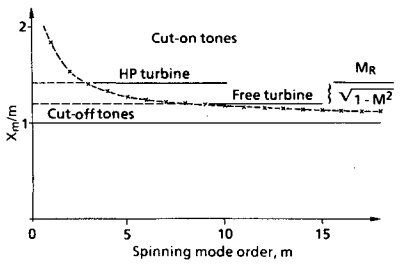


**Fig. 6 Prediction of the cut-on multiple pure tones generated by the TM 333 HP- and free-turbines.**

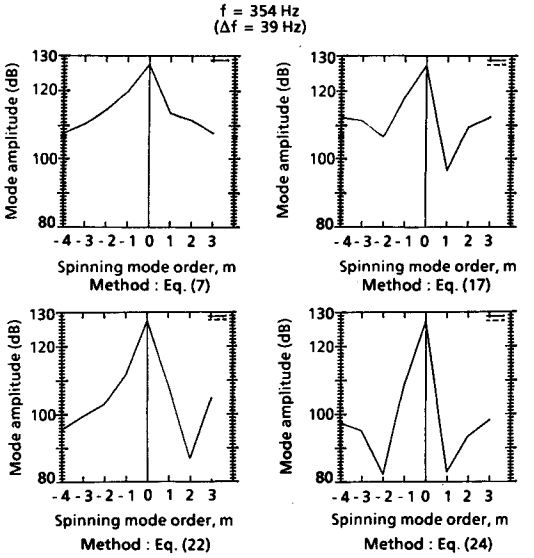


**Fig. 7 Wave number spectrum in the frequency range of combustion noise.**

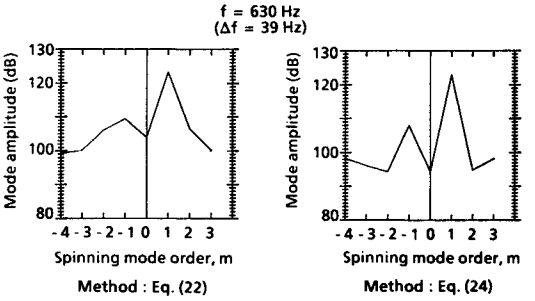


**Fig. 8 Wave number spectrum at the free-turbine rotation frequency, $f = N_{LP}$.**

Microphone $j = 1$ is taken as reference in the third method. The two small bars in the upper right corner of each spectrum mark 1) the total level in the frequency band $\Delta f$ (solid line); and 2) the coherent level, i.e., the sum of all the mode levels (dashed line).

The $(S/N)_{OUT}$ is obviously rather poor (on the order of 10 dB) in the first wave-number spectrum of Fig. 7, obtained by the conventional method. Only the two last spectra clearly show the plane wave ($m = 0$), which is the only cut-on mode because $f_c(1) = 970$ Hz.

The wave-number spectrum at the free-turbine rotation frequency, $f = N_{LP}$, is presented in Fig. 8, which clearly shows the mode $m = +1$, and also $m = -1$ with a much lower level. It is explained at the end of the previous section why these modes are observed although they are theoretically cut off. Note that the $m = -1$ levels are very close in both curves of Fig. 8. The method of Eq. (24) thus seems to lead to approximately the right levels even for the secondary modes since the $m = -1$ levels are very close in both curves. This means that the numerical simulation result of Fig. 2 is more severe than an actual test. The HP-turbine rotation frequency, $f = N_{HP}$, exhibits the same behavior (Fig. 9), but here $m = -1$ is the most intense.

Figure 10 shows the wave-number spectra for $f = 2N_{LP}$ and $f = 2N_{HP}$. Again, the $m = +2$ mode appears at $f = 2N_{LP}$ and $m = -2$ mode appears at $f = 2N_{HP}$ although their cut-on frequency $f_c(2) = 1607$ Hz is higher (the frequencies printed in the figures are the upper limits of the 39 Hz bands, and therefore may be slightly different from the peak frequencies). Figures 8–10 perfectly support the model given at the end of Sec. IV.A. The mode $m$ is generated at the frequency $f = mN$. However, the values of $m$ are positive for the free-turbine tones and negative for the HP-turbine tones. This is because the two turbines are counter-rotating, and emphasizes the

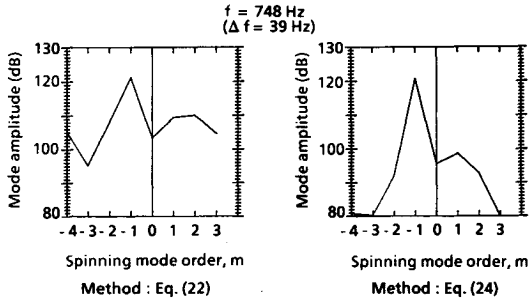


**Fig. 9 Wave number spectrum at the HP-turbine rotation frequency, $f = N_{HP}$.**

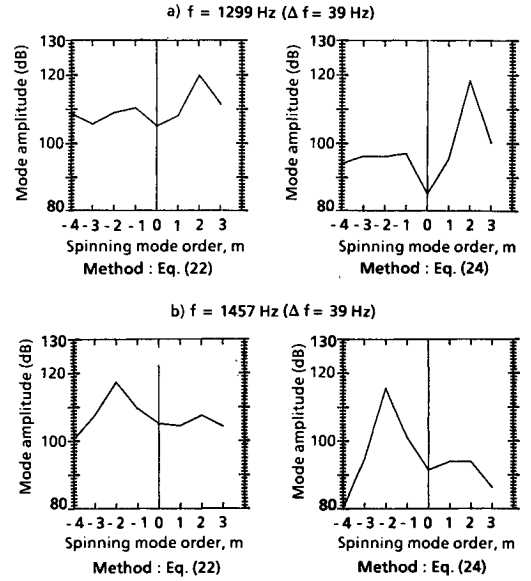


**Fig. 10 Wave number spectra at twice the shaft rotation speeds: a) first harmonic of the free-turbine rotation frequency, $f = 2N_{LP}$; and b) first harmonic of the HP-turbine rotation frequency, $f = 2N_{HP}$.**

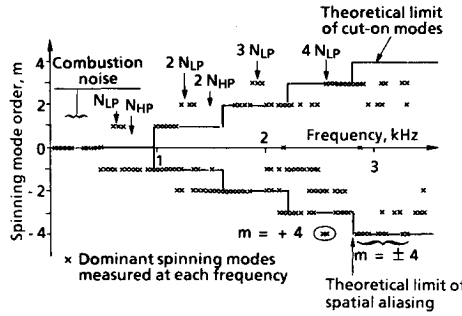


**Fig. 11 Synthesis of the dominant spinning modes measured in the TM 333 nozzle.**

importance of discriminating plus and minus signs in the wave-number spectra.

Finally, Fig. 11 is a synthesis of the experimental results. The main modes in each wave-number spectrum are plotted vs the frequency. The frequency range studied here is determined by the spatial aliasing problem appearing above 2.8 kHz since $m = +4$ is mixed with $m = -4$ (see Sec. IV.A.). In fact, the mode at $f = 4N_{LP} \simeq 2520$ Hz is $m = +4$ instead of $m = -4$. The prediction of the cut-on modes is well validated, but some modes ($m = -1, -2$) exist slightly below their cut-off frequencies, for reasons explained at the end of Sec. IV.A. The HP-turbine modes are not clearly seen in Fig. 11 because the same modes are emitted in a broadband frequency range around the HP-turbine tones, but the tone levels are much higher. It can also be noticed that the predominant modes are generally at the cut-on boundary (intense plane waves, $m = 0$, are only observed at low frequencies). This may be due to the acoustic impedance of near cut-off modes. It is also explained by the fact that the radial mode of these spinning waves is necessarily the lowest one, and the radial profile is then concentrated at the wall in a perfectly rigid duct. These modes are well detected because the measurements are made on the nozzle wall.

The above discussions give some examples of the information obtained by the spinning mode analysis. Further study of the actual noise sources would be needed to better explain the dominating modes in various frequency ranges. Another application is to use these data as input for prediction programs to determine the directivity pattern of the radiated noise, as was done for turbojet engines in Ref. 20.

## V. Conclusion

The spinning-mode structure of the acoustic field in a Turbomeca TM 333 turboshaft engine was determined using an angular array of fixed microphones in the nozzle. Data processing must deal with the high background noise due to the very turbulent internal flow. Several methods have been tested by numerical simulations.

1) The conventional method is based on the angular Fourier transform of the cross-spectral matrix, but the output noise remains rather high.

2) A first improvement consists in reducing the diagonal noise terms in the cross-spectral matrix by a three-signal coherence technique.

3) It seems to be slightly better to only process one line vector of the cross-spectral matrix 2), i.e., the cross-spectrum components between the various microphones and a reference one. A similar technique is used in our studies on turbofan engines, with a reference microphone and a slowly rotating probe.

4) A further step consists of reducing the nondiagonal noise terms generated by the estimate bias due to finite number of statistical averages. This is achieved by processing the mean value of the above line vectors, each of them being computed with another microphone taken as a reference.

In the present state, the second and third methods lead to the best wave-number spectra, with a good signal-to-noise ratio. The experimental results in the TM 333 correctly yield the theoretical cut-off properties introduced by the nozzle, and the predicted noise generation by the two transonic turbines. The discrimination between positive and negative modes helps to separate the tones emitted by the two turbines, since they are counter-rotating.

The work in progress now is twofold:

1) The fourth method described above gives a very low output noise, but the quantitative mode levels are not ascertained. Some modifications have already been tested, which seem to give more reliable results.

2) The experimental wave-number spectra will be entered as input data into computer programs predicting the free-field directivity of the radiated noise.

## Acknowledgments

This work was supported by a contract with the Service Technique des Programmes Aéronautiques and the Turbomeca Company. The authors thank A. Farrando, P. Jourbert, and all the staff of the Turbomeca open-air facility for their help, which made the tests possible. They also thank A. Guédel for having initiated the tests, G. Elias for many fruitful discussions, and R. Jean who implemented the special microphone probes.

## References

[1]Damongeot, A., d'Ambra, F., and Masure, B., "Towards a Better Understanding of Helicopter External Noise," *Proceedings of the 39th*

*Annual Forum of the American Helicopter Society,* St. Louis, MO, May 1983, pp. 445–457.

[2]Janakiram, R. D., Smith, M. J., and Tadghighi, H., "Importance of Engine as a Source of Helicopter External Noise," AIAA Paper 89-1147, San Antonio, TX, April 1989.

[3]Lévy, S., "Recent Research on External Helicopter Noise at ONERA," *Vertiflite,* Vol. 35, Nov.–Dec. 1989, pp. 56–61.

[4]Guédel, A., and Farrando, A., "Turboshaft Engine Noise Study," *Proceedings of the 14th Congress of the International Council of the Aeronautical Sciences,* Vol. 2, Toulouse, France, Sept. 1984, pp. 989–995.

[5]Guédel, A., and Farrando, A., "Experimental Study of Turboshaft Engine Core Noise," *Journal of Aircraft,* Vol. 23, No. 10, 1986, pp. 763–767.

[6]Tyler, J.M., and Sofrin, T. G., "Axial Flow Compressor Noise Studies," *Society of Automotive Engineers Transactions*, Vol. 70, 1962, pp. 309–332.

[7]Mugridge, B. D., "The Measurement of Spinning Acoustic Modes Generated in an Axial Flow Fan," *Journal of Sound and Vibration,* Vol. 10, No. 2, 1969, pp. 227–246.

[8]Bolleter, U., and Crocker, M. J., "Theory and Measurement of Modal Spectra in Hard-Walled Cylindrical Ducts," *Journal of the Acoustical Society of America,* Vol. 51, No. 5, Pt. 1, May 1972, pp. 1439–1447.

[9]Harel, P., and Pérulli, M., "Measurement, in a Duct, of the Space-Structure of the Discrete-Frequency Noise Generated by an Axial Compressor," *Journal of Sound and Vibration,* Vol. 23, No. 4, 1972, pp. 487–506.

[10]Lévy, S., Canard-Caruana, S., and Julliard, J., "Experimental Study of Noise Sources and Acoustic Propagation in a Turbofan Model," AIAA Paper 90-3950, Tallahassee, FL, Oct. 1990.

[11]Kraft, R. E., Paas, J. E., and Clark, L. R., "Effects of Multi-Element Acoustic Treatment on Compressor Inlet Noise," AIAA Paper 76-515, Palo Alto, CA, July 1976.

[12]Joppa, P. D., "Acoustic Mode Measurements in the Inlet of a Turbofan Engine," *Journal of Aircraft,* Vol. 24, No. 9, 1987, pp. 587–593.

[13]Sofrin, T. G., and Cicon, D. E., "Ducted Fan Noise Propagation in Non-Uniform Flow—Part I: Test Background and Simplified Model," AIAA Paper 87-2701, Sunnyvale, CA, Oct. 1987.

[14]Sofrin, T. G., and Cicon, D. E., "Ducted Fan Noise Propagation in Non-Uniform Flow—Part II: Wave Equation Solution," AIAA Paper 87-2702, Sunnyvale, CA, Oct. 1987.

[15]Nakamura, Y., and Isomura, K., "Detection of Fan Acoustic Modes," AIAA Paper 87-2700, Sunnyvale, CA, Oct. 1987.

[16]Bendat, J. S., and Piersol, A. G., *Engineering Applications of Correlation and Spectral Analysis,* Wiley, New York, 1980, Chap. 8, pp. 188–209.

[17]Lévy, S., Canard, S., and Kerviel, P., "Study of Propagating Acoustic Sources in a Fan Intake by Modal Analysis of Tone Noise," *Proceedings of Inter-Noise 88,* Avignon, France, SFA & Noise Control Foundation, Vol. 2, Aug.–Sept. 1988, pp. 751–754.

[18]Farrando, A., "Helicopter Turboshaft Engine Acoustic and Infrared Studies and Tests," 12th European Rotorcraft Forum, Paper 87, Sept. 1986.

[19]Benzakein, M. J., Kazin, S. B., and Savell, C. T., "Multiple Pure Tone Noise Generation and Control," AIAA Paper 73-1021, Seattle, WA, Oct. 1973.

[20]Lévy, S., "Exact and Simplified Computation of Noise Radiation by an Annular Duct," *Proceedings of Inter-Noise 88,* Avignon, France, SFA & Noise Control Foundation, Vol. 3, Aug.–Sept. 1988, pp. 1559–1564.